Hydrogen-induced changes in the properties of Zr-based AB_2 alloy studied by x-ray, electrical resistivity and differential scanning calorimetry

2006 J. Phys.: Condens. Matter 18 2943

(http://iopscience.iop.org/0953-8984/18/11/002)

INSTITUTE OF PHYSICS PUBLISHING JOURNAL OF PHYSICS: CONDENSED MATTER

J. Phys.: Condens. Matter **18** (2006) 2943–2954 doi:10.1088/0953-8984/18/11/002

Hydrogen-induced changes in the properties of Zr-based AB_2 alloy studied by x-ray, electrical resistivity and differential scanning calorimetry

M Kandavel and S Ramaprabhu[1]

Alternative Energy Technology Laboratory, Department of Physics, Indian Institute of Technology Madras, Chennai-600 036, India

E-mail: ramp@iitm.ac.in

Received 15 August 2005, in final form 19 January 2006
Published 27 February 2006
Online at stacks.iop.org/JPhysCM/18/2943

Abstract

Powder x-ray diffraction and the electrical resistivity of $(Ti_{0.1}Zr_{0.9})_{1.1}Mn_{0.9}V_{0.1}Fe_{0.5}Ni_{0.5}$–$H_x$ with different hydrogen concentrations have been investigated and the results have been discussed. An experimental facility has been developed to measure the *in situ* electrical resistivity of alloys during the hydrogen absorption process. Variation in *in situ* electrical resistivity with hydrogen concentration in $(Ti_{0.1}Zr_{0.9})_{1.1}Mn_{0.9}V_{0.1}Fe_{0.5}Ni_{0.5}$ has been explained using the phase transformation during hydrogen absorption. Differential scanning calorimetry (DSC) studies have been performed in $(Ti_{0.1}Zr_{0.9})_{1.1}Mn_{0.9}V_{0.1}Fe_{0.5}Ni_{0.5}$–$H_x$ with different hydrogen concentrations in the temperature range 50–250 °C under argon atmosphere. The DSC studies show that the desorption of hydrogen is from the $24l$ (A_2B_2) tetrahedral sites. The activation energies and diffusion coefficients of hydrogen in $(Ti_{0.1}Zr_{0.9})_{1.1}Mn_{0.9}V_{0.1}Fe_{0.5}Ni_{0.5}$ have been determined in the range 30–100 °C from the hydrogen absorption kinetics measurements. The diffusion coefficient of hydrogen in $(Ti_{0.1}Zr_{0.9})_{1.1}Mn_{0.9}V_{0.1}Fe_{0.5}Ni_{0.5}$–$H_x$ at 30 °C is 1.1×10^{-10} cm^2 s^{-1}.

1. Introduction

Metal hydrides are of considerable interest for safe and practical hydrogen storage. Among the different types of metal hydrides, Zr-based AB_2 Laves phases are regarded as promising hydrogen storage materials for vehicular applications due to their high storage capacity, fast kinetics and easy activation [1–3]. From our previous study, we identified the presence of different phases in Zr-based AB_2 Laves phase hydrides from the kinetics of hydrogen absorption, x-ray diffraction with different hydrogen concentration [4]. However, the measurements of electrical resistivity during hydrogen absorption in alloys are difficult because

[1] Author to whom any correspondence should be addressed.

of the decrepitation of alloys into fine particles during hydrogen absorption. Previous reports show that this problem can be overcome by using compressed powder [5] and thin films [6, 7]. However, Ishikawa *et al* [8] developed a new method to measure the *in situ* electrical resistivity of unstable $LaNi_5H_x$ and $LaCo_5H_x$. In order to restrain rapid volume expansion and prevent the sample from fracturing, the sample was allowed to react with hydrogen under the influence of mechanical stress. Moreover, differential scanning calorimetry has been used to study the various reactions taking place in alloy hydrides during heating [9, 10]. Fernandez *et al* have studied the hydrogen desorption and heat of formation simultaneously in Zr-based C15 Laves phase alloys using differential scanning calorimetry–mass spectrometry [11]. Aoki *et al* identified the preferential occupancy of hydrogen atoms in C15 Laves phase $GdFe_2$ alloy hydrides (A_2B_2 and AB_3) from the DSC studies of its hydrides [12].

Our earlier hydrogen absorption studies of stoichiometry and non-stoichiometry Zr-based AB_2 alloys revealed that the $(Ti_{0.1}Zr_{0.9})_{1.1}Mn_{0.9}V_{0.1}Fe_{0.5}Ni_{0.5}$ forms stable hydride at room temperature [4]. In this paper, we present the systematic study of the growth of different phases using powder x-ray diffraction of $(Ti_{0.1}Zr_{0.9})_{1.1}Mn_{0.9}V_{0.1}Fe_{0.5}Ni_{0.5}$–$H_x$ with different hydrogen concentrations. The dependence of electrical resistivity of $(Ti_{0.1}Zr_{0.9})_{1.1}Mn_{0.9}V_{0.1}Fe_{0.5}Ni_{0.5}$–$H_x$ on the hydrogen concentration and *in situ* electrical resistivity of $(Ti_{0.1}Zr_{0.9})_{1.1}Mn_{0.9}V_{0.1}Fe_{0.5}Ni_{0.5}$ have been studied using the linear four-probe method and the results have been discussed. DSC studies of $(Ti_{0.1}Zr_{0.9})_{1.1}Mn_{0.9}V_{0.1}Fe_{0.5}Ni_{0.5}$–$H_x$ have been performed in order to determine the nature of the desorption reaction and the hydrogen site occupancy. In addition, we present the results obtained from the kinetics of hydrogen absorption studies of $(Ti_{0.1}Zr_{0.9})_{1.1}Mn_{0.9}V_{0.1}Fe_{0.5}Ni_{0.5}$ in the temperature range 30–100 °C.

2. Experimental details

$(Ti_{0.1}Zr_{0.9})_{1.1}Mn_{0.9}V_{0.1}Fe_{0.5}Ni_{0.5}$ has been prepared by arc melting the high purity constituent elements with stoichiometric proportions in an arc furnace (∼0.80 bar Ar atmosphere). Since the vapour pressure of Mn is very high, 6 wt% of excess Mn is added to the total mixture following the normal procedure. The alloy button was then remelted six times by turning it upside down, after each solidification, to ensure homogeneity. The percentage weight loss of the alloy during the preparation was less than 0.2%. The alloy powders were activated towards hydrogen by exposing them to a hydrogen atmosphere of 20 bar at room temperature. Degassing was performed by heating the alloy hydride particles at 200 °C in vacuum. Alloy hydrides with different hydrogen concentrations for XRD, resistivity and DSC measurements were obtained, after six absorption/desorption cycles, by allowing different initial hydrogen gas pressures inside the sample chamber.

Room temperature powder x-ray diffraction patterns have been obtained for $(Ti_{0.1}Zr_{0.9})_{1.1}Mn_{0.9}V_{0.1}Fe_{0.5}Ni_{0.5}$–$H_x$ using Cu Kα radiation. Resistivity measurements of $(Ti_{0.1}Zr_{0.9})_{1.1}Mn_{0.9}V_{0.1}Fe_{0.5}Ni_{0.5}$–$H_x$ have been carried out using the linear four-probe method on pellets (8 mm × 2 mm) at room temperature. An experimental facility has been developed to measure the *in situ* resistivity of alloys during hydrogen absorption. The samples for *in situ* resistivity measurements have been obtained by completely degassing the alloy hydrides after six hydrogen absorption/desorption cycles. These alloy particles were then compressed in the form of pellets with dimensions of 8 mm diameter and 2 mm thickness. A block diagram of the experimental facility (sample holder) developed is shown in figure 1, where the pellet was tightly packed with silica powder. This compression can prevent further fracturing of alloy particles during hydrogen absorption. Moreover, silica powders easily allow the hydrogen gas molecules to pass through because of the small size of hydrogen molecules. The sample holder

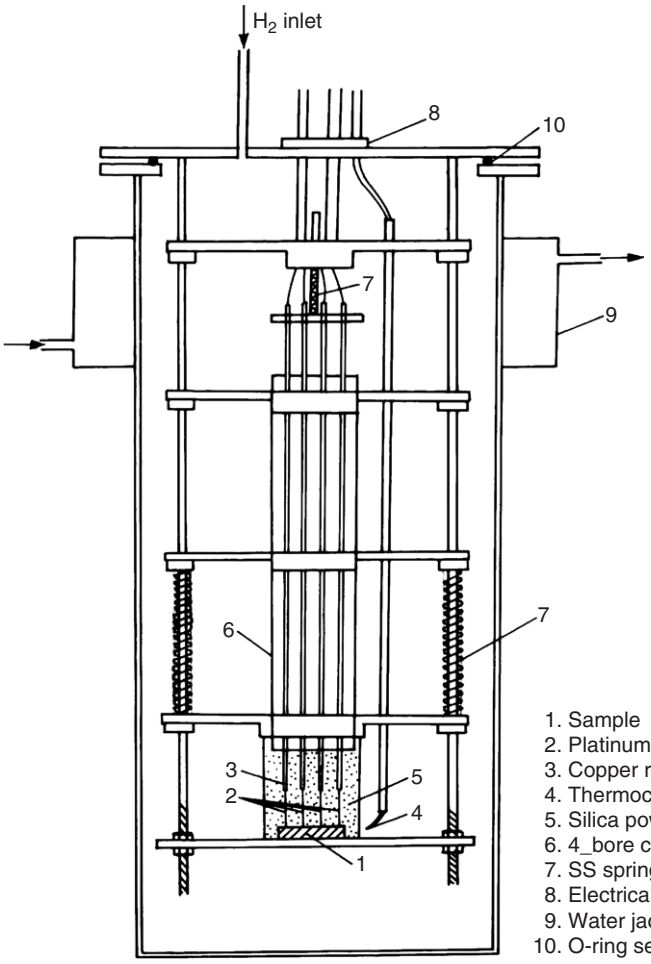

Figure 1. A block diagram of the sample holder for *in situ* resistivity measurement of alloy hydrides.

was then placed in a closed chamber and the sample was allowed to react with hydrogen. Electrical resistivity was then measured by the linear four-probe method during the hydrogen absorption process. The differential scanning calorimetry analyses have been performed with 10 mg of alloy hydride powder with a heating rate of 10 °C min^{-1} under an argon flow rate of 100 ml min^{-1}.

3. Results and discussion

3.1. XRD studies

The room temperature powder x-ray diffraction patterns of $(Ti_{0.1}Zr_{0.9})_{1.1}Mn_{0.9}V_{0.1}Fe_{0.5}Ni_{0.5}$–$H_x$ with different hydrogen concentrations are shown in figure 2. The XRD pattern of pure alloy shows that this alloy crystallizes in the C14 hexagonal structure with space group $P6_3/mmc$ and the corresponding diffraction peaks are indexed. As the hydrogen concentration increases up to $x = 0.6$, the diffraction peaks of the hydrides are identical to that of the parent alloy with small changes in the lattice parameters and the intensity of the diffraction peaks decreases (α phase). As the hydrogen concentration increases beyond $x = 0.6$, a new set of Bragg reflections starts appearing. These reflections grow as the amount of hydrogen

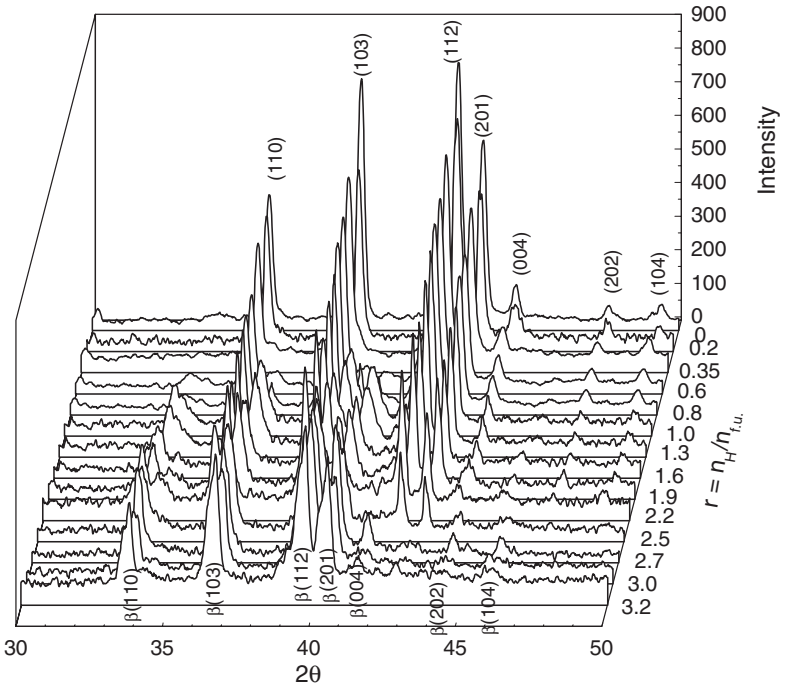

Figure 2. Powder x-ray diffraction patterns of $(Ti_{0.1}Zr_{0.9})_{1.1}Mn_{0.9}V_{0.1}Fe_{0.5}Ni_{0.5}$–$H_x$ ($x = 0$, 0.2, 0.35, 0.6, 0.8, 1.0, 1.3, 1.6, 1.9, 2.2, 2.5, 2.7, 3.0 and 3.2).

concentration increases. The new set of Bragg reflections is identical to that of parent alloy with a large shift towards the lower angle. These reflections are due to the formation of hydride phase (β phase) with increase in hydrogen concentration. The intensity of these reflections corresponding to the β phase increases and simultaneously the intensity of the reflections corresponding to the α phase decreases with hydrogen concentration. This may be due to the growth of the hydride phase (β phase) at the expense of metal rich phase (α phase). When the hydrogen concentration is around 2.7, Bragg reflections corresponding to the α phase disappear, revealing the complete formation of the alloy hydride phase. The phase regions and phase boundaries identified using the above XRD analysis are in good agreement with those identified from the pressure–composition (P–C) isotherms at 30 °C (figure 3). Figure 4 shows the intensity variation of the (112) peak with hydrogen concentration in the α and β phases in $(Ti_{0.1}Zr_{0.9})_{1.1}Mn_{0.9}V_{0.1}Fe_{0.5}Ni_{0.5}$–$H_x$. Lattice parameters and unit cell volumes of the α phase and β phase have been obtained using the least square refinement technique and are given in table 1. The volume expansion with maximum hydrogen concentration is found to be around 26%.

3.2. Resistivity of alloy hydrides

Electrical resistivities of alloy hydrides have been studied using the linear four-probe method. Pellets of dimensions 8 mm × 2 mm were used for the measurements. The main factors affecting the electrical resistivity are the particle size and density of the pellets. Previous hydrogen absorption studies showed that the particle size becomes uniform after several hydrogen absorption/desorption cycles [13]. The relation between the rate of hydrogen

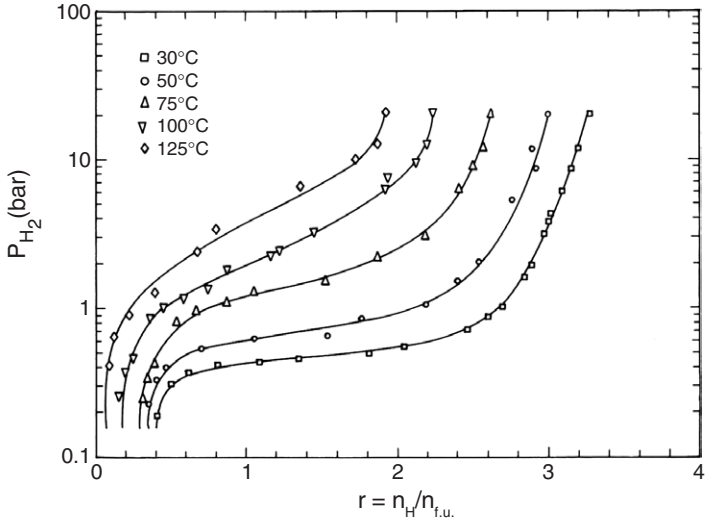

Figure 3. Pressure–composition (P–C) isotherms of $(Ti_{0.1}Zr_{0.9})_{1.1}Mn_{0.9}V_{0.1}Fe_{0.5}Ni_{0.5}$.

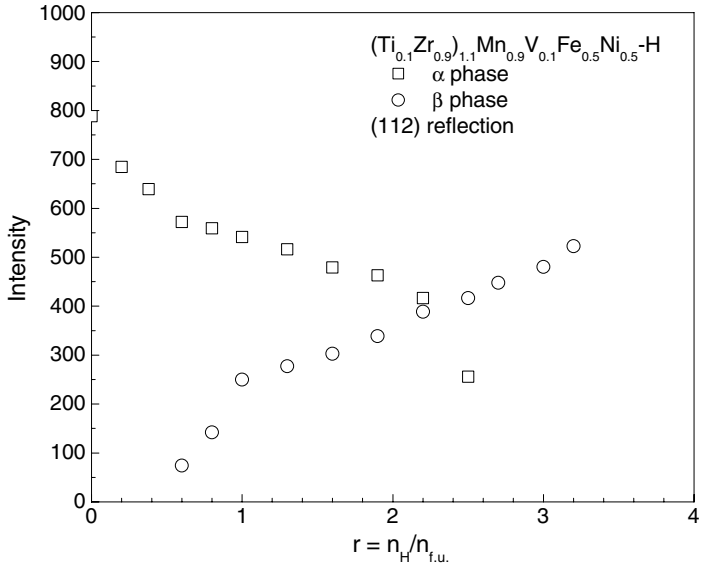

Figure 4. Variation of the intensity of (112) reflection in the α phase and β phase with hydrogen concentration in $(Ti_{0.1}Zr_{0.9})_{1.1}Mn_{0.9}V_{0.1}Fe_{0.5}Ni_{0.5}$–$H_x$.

absorption and the number of cycles is that when the time required for two consecutive absorption cycles is the same then the activation is complete. Thereafter, the particle size remains uniform [14]. In the present study, the alloy hydrides for resistivity measurements have been obtained after six hydrogen absorption/desorption cycles. Pellets of these alloy hydrides have been obtained by applying uniform load (about 5 t) and the mean value of density of the alloy hydride pellets is 6.53 g cm^{-3}. Figure 5 shows the variation of electrical resistivity of $(Ti_{0.1}Zr_{0.9})_{1.1}Mn_{0.9}V_{0.1}Fe_{0.5}Ni_{0.5}$–$H_x$ at room temperature with hydrogen concentration. The variation shows an increase–decrease–increase behaviour of electrical resistivity. This

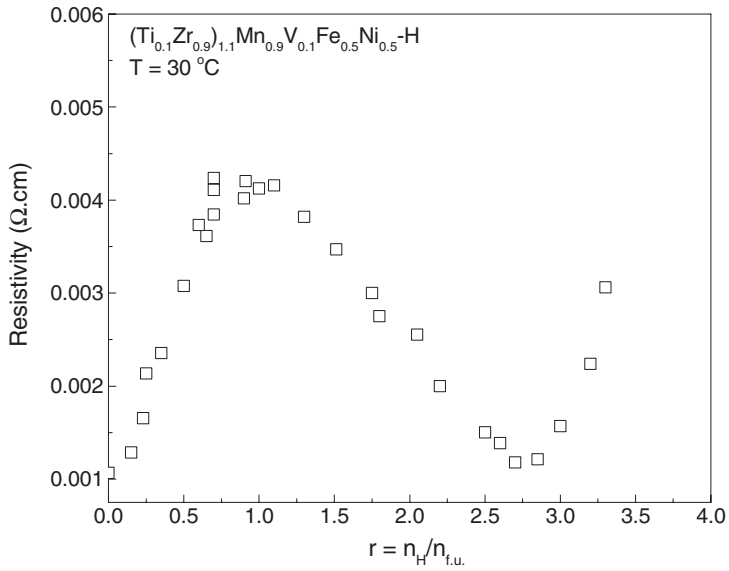

Figure 5. Resistivity versus hydrogen concentration plot for $(Ti_{0.1}Zr_{0.9})_{1.1}Mn_{0.9}V_{0.1}Fe_{0.5}Ni_{0.5}$–$H_x$.

Table 1. Lattice parameters and unit cell volumes of $(Ti_{0.1}Zr_{0.9})_{1.1}Mn_{0.9}V_{0.1}Fe_{0.5}Ni_{0.5}$–$H_x$.

$R = n_H/n_{f.u.}$	a (Å)	c (Å)	v (Å^3)	$\Delta v/v$ (%)
0	$4.992 \pm 0.002(\alpha)$	$8.148 \pm 0.002(\alpha)$	$175.8 \pm 0.1(\alpha)$	0
0.2	$5.000 \pm 0.002(\alpha)$	$8.172 \pm 0.004(\alpha)$	$176.9 \pm 0.2(\alpha)$	0.6
0.35	$5.004 \pm 0.001(\alpha)$	$8.190 \pm 0.004(\alpha)$	$177.6 \pm 0.1(\alpha)$	1.0
0.6	$5.007 \pm 0.003(\alpha)$	$8.186 \pm 0.006(\alpha)$	$177.6 \pm 0.3(\alpha)$	1.0
	$5.321 \pm 0.007(\beta)$	$8.652 \pm 0.009(\beta)$	$212.2 \pm 0.6(\beta)$	20.7
0.8	$5.007 \pm 0.001(\alpha)$	$8.183 \pm 0.002(\alpha)$	$177.7 \pm 0.1(\alpha)$	1.1
	$5.322 \pm 0.006(\beta)$	$8.659 \pm 0.009(\beta)$	$212.5 \pm 0.6(\beta)$	20.8
1.0	$5.000 \pm 0.002(\alpha)$	$8.174 \pm 0.002(\alpha)$	$177.0 \pm 0.1(\alpha)$	0.7
	$5.326 \pm 0.006(\beta)$	$8.716 \pm 0.008(\beta)$	$214.1 \pm 0.5(\beta)$	21.8
1.3	$5.000 \pm 0.001(\alpha)$	$8.174 \pm 0.002(\alpha)$	$177.0 \pm 0.1(\alpha)$	0.7
	$5.330 \pm 0.008(\beta)$	$8.714 \pm 0.009(\beta)$	$214.4 \pm 0.8(\beta)$	21.9
1.6	$5.002 \pm 0.001(\alpha)$	$8.178 \pm 0.001(\alpha)$	$177.2 \pm 0.1(\alpha)$	0.8
	$5.333 \pm 0.009(\beta)$	$8.720 \pm 0.009(\beta)$	$214.8 \pm 0.8(\beta)$	22.2
1.9	$5.008 \pm 0.003(\alpha)$	$8.181 \pm 0.005(\alpha)$	$177.7 \pm 0.3(\alpha)$	1.1
	$5.345 \pm 0.006(\beta)$	$8.701 \pm 0.008(\beta)$	$215.3 \pm 0.5(\beta)$	22.4
2.2	$5.008 \pm 0.002(\alpha)$	$8.181 \pm 0.004(\alpha)$	$177.7 \pm 0.2(\alpha)$	1.1
	$5.345 \pm 0.007(\beta)$	$8.721 \pm 0.008(\beta)$	$215.8 \pm 0.6(\beta)$	22.7
2.5	$5.011 \pm 0.003(\alpha)$	$8.199 \pm 0.005(\alpha)$	$178.3 \pm 0.3(\alpha)$	1.4
	$5.355 \pm 0.009(\beta)$	$8.743 \pm 0.007(\beta)$	$217.2 \pm 0.8(\beta)$	23.5
2.7	$5.361 \pm 0.009(\beta)$	$8.772 \pm 0.009(\beta)$	$218.3 \pm 0.8(\beta)$	24.2
3.0	$5.364 \pm 0.007(\beta)$	$8.764 \pm 0.009(\beta)$	$218.4 \pm 0.7(\beta)$	24.2
3.2	$5.391 \pm 0.008(\beta)$	$8.793 \pm 0.008(\beta)$	$221.3 \pm 0.7(\beta)$	25.9

behaviour can be explained using different phases present in the alloy hydride system. The initial increase in electrical resistivity with increase in hydrogen concentration is due to the hydrogen atoms in the α phase acting as scattering centres for the electron flow and thereby

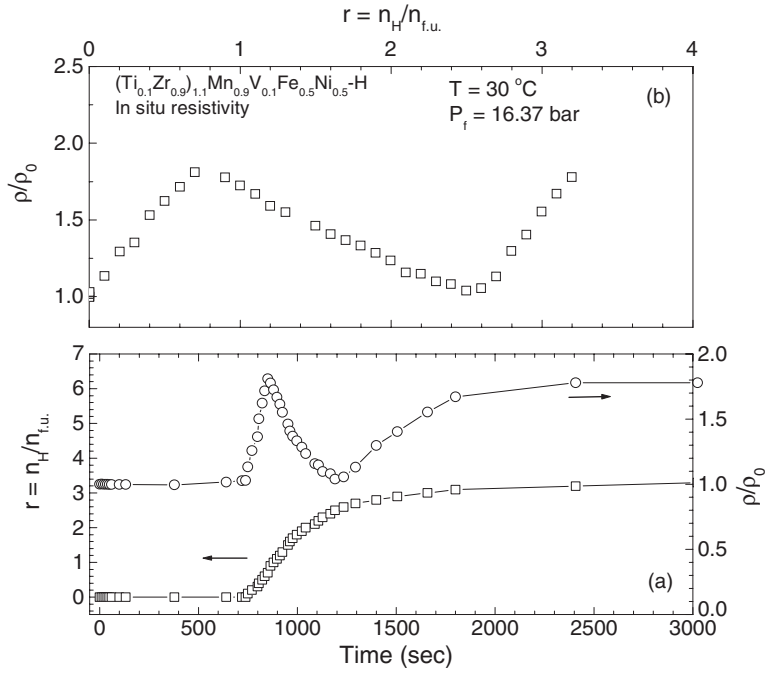

Figure 6. (a) Variation of ρ/ρ_0 and hydrogen concentration with time and (b) *in situ* ρ/ρ_0 variation with hydrogen concentration during hydrogen absorption at room temperature for $(Ti_{0.1}Zr_{0.9})_{1.1}Mn_{0.9}V_{0.1}Fe_{0.5}Ni_{0.5}$.

induces an increase in resistivity. Further increase in hydrogen concentration leads to the formation of clusters of hydrogen atoms ($\alpha + \beta$ phase), which effectively reduces the number of hydrogen scattering centres. This reduction in the scattering centres leads to an increase in electrical conductivity and thereby a decrease in resistivity is observed in the concentration range $x = 0.7$–2.7. As the hydrogen concentration increases beyond $x = 2.7$, there is an increase in resistivity observed. This may be due to the random arrangement of hydrogen atoms in the metal hydride phase acting as a scattering centre for the electron flow and thereby resulting in increased resistivity with hydrogen concentration.

3.3. In situ resistivity studies

Figure 6(a) shows the variation of ρ/ρ_0 ($\rho_0 = 2.7 \times 10^{-3}$ Ω cm) and hydrogen concentration with time during hydrogen absorption at room temperature for $(Ti_{0.1}Zr_{0.9})_{1.1}Mn_{0.9}V_{0.1}Fe_{0.5}Ni_{0.5}$. The ρ/ρ_0 value as well as hydrogen concentration suddenly started to increase after 10 min of hydrogen charging and reaches an equilibrium value, which is due to the formation of hydrides. There is an anomaly in the resistivity variation; first a maximum and then a minimum of ρ/ρ_0 takes place at different times. The real task is the explanation of the non-monotonic change in the resistivity with time. In order to explain this anomalous behaviour, we have plotted the dependence of ρ/ρ_0 with hydrogen concentration and this is shown in figure 6(b). The variation shows an increase–decrease–increase behaviour of ρ/ρ_0. It seems this variation is due to enhanced electron scattering by the hydrogen interstitial atoms in the α and β phases. The dependence of *in situ* electrical resistivity with hydrogen concentration is similar to the electrical resistivity of the alloy hydrides. For the concentration

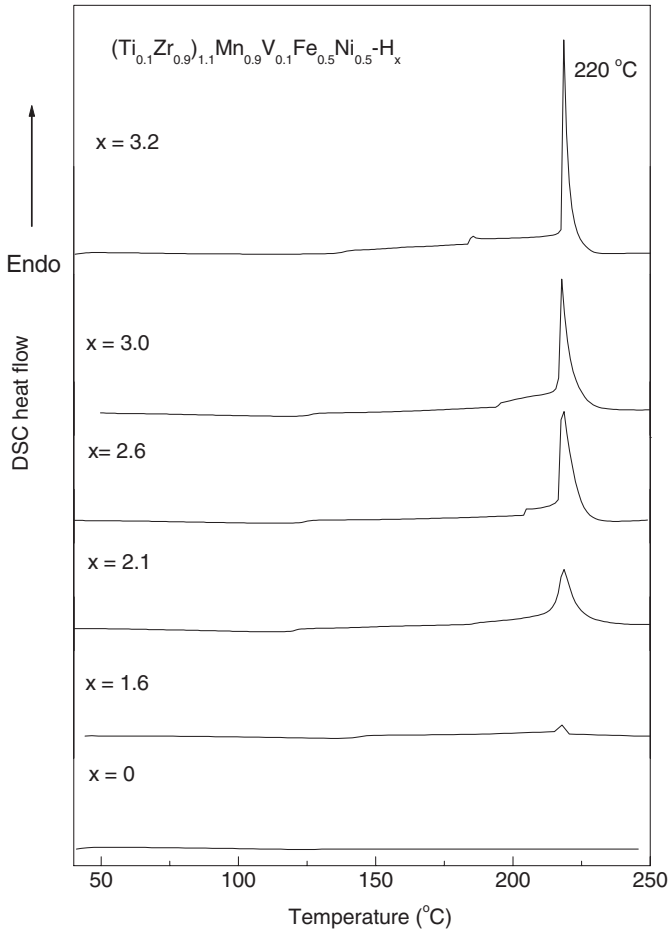

Figure 7. DSC curves of $(Ti_{0.1}Zr_{0.9})_{1.1}Mn_{0.9}V_{0.1}Fe_{0.5}Ni_{0.5}$–$H_x$ with different hydrogen concentrations.

range $x = 0$–0.7, random occupation of hydrogen atoms in the interstitial sites leads to an increase in the electrical resistivity. For $x = 0.7$–2.6, cluster formation of hydrogen atoms occurs, which effectively reduces the number of scattering centres and thereby a decrease in resistivity is observed. As the hydrogen concentration increases beyond $x = 2.6$, the increase in resistivity is due to randomly arranged hydrogen atoms in the metal hydride phase acting as scattering centres for the electron flow. Different phases and phase boundaries obtained from the *in situ* resistivity measurement is in good agreement with those identified from *P–C* isotherms at 30 °C (figure 3) and resistivity of alloy hydrides (figure 5).

3.4. DSC studies

Desorption of hydrogen from $(Ti_{0.1}Zr_{0.9})_{1.1}Mn_{0.9}V_{0.1}Fe_{0.5}Ni_{0.5}$–$H_x$ with different hydrogen concentration has been analysed using differential scanning calorimetry (DSC). DSC experiments have been performed with 10 mg of alloy hydride powder with heating rate of 10 °C min^{-1} under the argon flow rate of 100 ml min^{-1}. After six hydrogen absorption/desorption cycles, the alloy hydride powders were taken out from the

sample cell and used for DSC measurements. Figure 7 shows the DSC curves of $(Ti_{0.1}Zr_{0.9})_{1.1}Mn_{0.9}V_{0.1}Fe_{0.5}Ni_{0.5}$–$H_x$ with different hydrogen concentrations. All DSC curves of the alloy hydrides show a strong endothermic peak in the temperature range 215–220 °C. It is reported that, in C15 Laves phase $GdFe_2$–H_x, hydrogen atoms can occupy two tetrahedral sites, namely A_2B_2 and AB_3. DSC curves of $GdFe_2$–H_x also show two endothermic peaks corresponding to A_2B_2 and AB_3 sites [12]. In our case we observed one major endothermic peak at around 220 °C. This may be due to desorption of hydrogen atoms from the stronger energy site in the C14 structure. In C14 Laves phase AB_2 alloys there are different interstitial sites available for hydrogen occupancy such as A_2B_2, AB_3 and B_4. Previous neutron diffraction studies of C14 Laves phase alloys revealed that the preferential occupancy of hydrogen atoms in C14 Laves phases is only different types of A_2B_2 sites, and the other tetrahedral sites such as AB_3 and B_4 are not preferred [15]. This implies that the strong endothermic peak observed in $(Ti_{0.1}Zr_{0.9})_{1.1}Mn_{0.9}V_{0.1}Fe_{0.5}Ni_{0.5}$–$H_x$ may be due to desorption of hydrogen from the 24*l* (A_2B_2) tetrahedral sites. However, in addition to a strong peak around 220 °C, we also observe a small kink at lower temperature. This can be explained due to breaking of the oxide layer covering the small particles forming the sample as explained in [11]. During the transfer of metal hydride particles to the DSC unit, there may be surface oxidation that gives rise to stabilization of the hydrides. During the thermal heating, hydrogen can diffuse through the oxide layer and evolve from the sample. This process is usually slow because of the low diffusivity of hydrogen through the oxide layer, and after the diffusion process it recombines at the surface and then H_2 desorption proceeds faster, which will be observed as a sudden increase in the DSC curves [11].

3.5. Kinetics of hydrogen absorption

The kinetics of hydrogen absorption has been obtained by measuring the hydrogen pressure change during the hydrogen absorption process in a closed system of constant volume. It would appear that the absorption rate is controlled by different mechanisms when the reactions proceed through different phase regions. The possible rate determining steps involved in the hydrogen absorption kinetics are the surface process, the interface process and diffusion. The surface process, chemisorption and nucleation of the hydrides occur at the initial stage of absorption. As the absorption process proceeds further, the hydride phase nuclei start growing. After some time, the growing hydride phase nuclei contact with each other with a corresponding decrease in interfacial area and in this process the reaction rate is controlled by the phase transformation at the $\alpha \rightarrow \beta$ interface [16]. When the β phase hydride is formed completely, the diffusion of hydrogen should constitute the rate determining step [17, 18].

Figure 8 shows the typical measurement of the kinetics of hydrogen absorption of $(Ti_{0.1}Zr_{0.9})_{1.1}Mn_{0.9}V_{0.1}Fe_{0.5}Ni_{0.5}$ at different temperatures. It can be seen that the hydrogen concentration increases with time and reaches an equilibrium concentration. The hydrogen absorption reaction rate increases with increase in temperature, which is attributed to the diffusion controlled reaction. The experimental data have been analysed using the Avrami–Erofeev rate equation

$$F = 1 - e^{-kt^n} \tag{1}$$

where F is the fractional hydrogen concentration in the host alloy, k is the reaction constant and n is the reaction order. To determine the reaction order, the experimental data can be analysed with the following method. When the order is assumed, the rate equation which best fits the observed data can be found for the appropriate value of the order (n). For our systems, the reaction order was determined as 1.0 for all phases by fitting the experimental data. Therefore

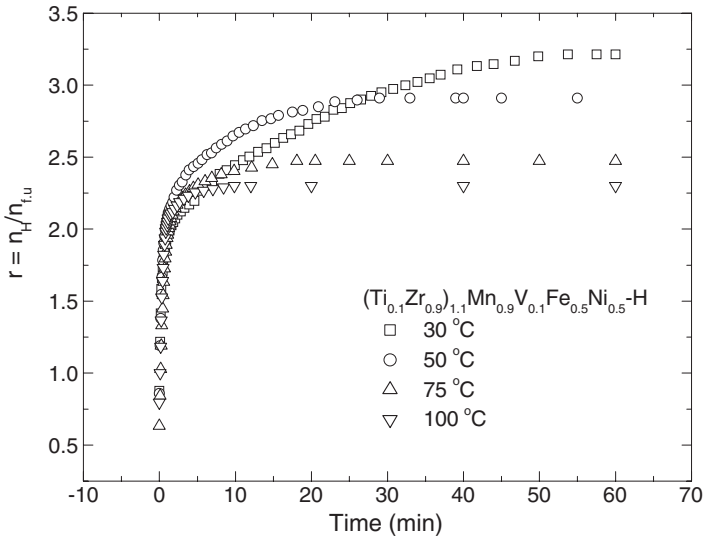

Figure 8. The hydrogen absorption kinetics of $(Ti_{0.1}Zr_{0.9})_{1.1}Mn_{0.9}V_{0.1}Fe_{0.5}Ni_{0.5}$ at different temperatures.

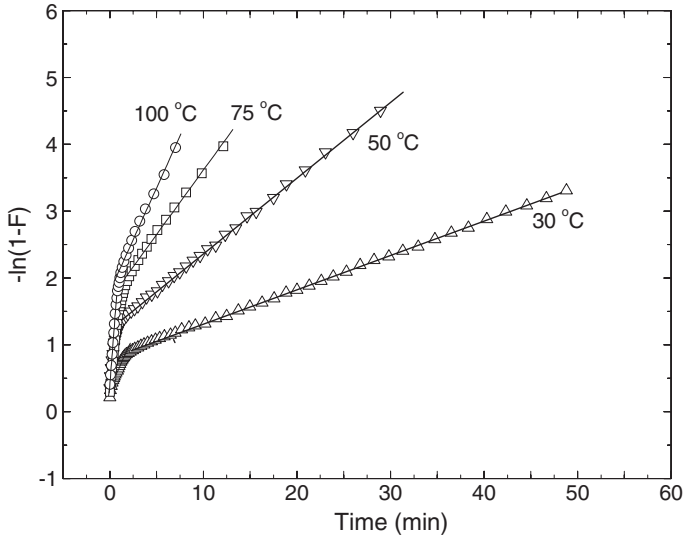

Figure 9. $-\ln(1-F)$ versus t plot for $(Ti_{0.1}Zr_{0.9})_{1.1}Mn_{0.9}V_{0.1}Fe_{0.5}Ni_{0.5}$–H at different temperatures.

the rate equation becomes

$$-\ln(1-F) = kt. \tag{2}$$

To obtain reaction constants k using equation (2), the results of the hydrogen absorption process for various constant temperatures are plotted as $-\ln(1-F)$ versus t. It may be seen from figure 9 that the experimental data fit to two linear segments and a gradual slope change occurs. This implies that two different processes are controlling the rate at initial and final stages of the absorption reaction respectively. It was found from the P–C isotherms that the concentration

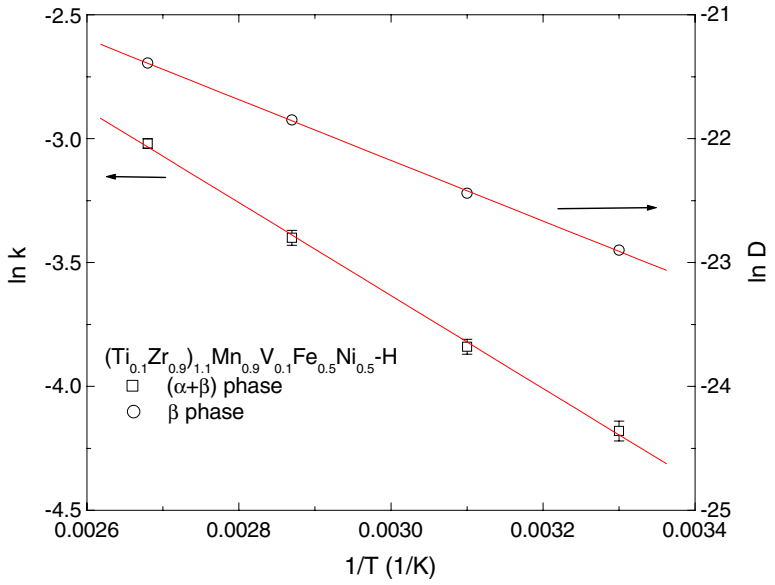

Figure 10. $\ln k$ versus $1/T$ and $\ln D$ versus $1/T$ plots in the $\alpha + \beta$ phase and β phase for the $(Ti_{0.1}Zr_{0.9})_{1.1}Mn_{0.9}V_{0.1}Fe_{0.5}Ni_{0.5}$–H.

(This figure is in colour only in the electronic version)

at which the slope changes corresponds to the $\alpha + \beta$ phase to β phase transition region [19]. The first linear segment would seem to correspond to the $\alpha + \beta$ phase and the second one to the β phase. The surface process, chemisorption and nucleation of the hydrides occur at the initial stage of absorption, which seem to be unnoticed in our case, because of the fast reaction kinetics in the α phase. The rate constants (k) have been calculated for the $\alpha + \beta$ phase and β phase at various temperatures from the slopes of the first and second linear regions of the fit shown in figure 9 respectively.

When the β phase hydride is formed completely, the diffusion of hydrogen will be the rate determining step [17]. It is possible to determine the diffusion coefficient (D) from the rate constant of the diffusion controlled reaction. The hydrogen diffusion coefficient can be obtained for the hydrogen content m_t at time t with a spherical particle of radius r from the first term of the series expansion of Fick's second law [20, 21]

$$1 - \frac{m_t}{m_\infty} = \frac{6}{\pi^2} \sum_{l=1}^{\infty} \frac{1}{l^2} \exp\left(\frac{-l^2\pi^2 Dt}{r^2}\right). \tag{3}$$

For $l = 1$, equation (3) is similar to (2). The diffusion coefficients have been calculated from the slope ($K_D = \frac{\pi^2 D}{r^2}$) of the linear region ($\beta$-phase) of the $-\ln(1 - F)$ versus t plot (figure 9) using an average particle radius r [4]. From our earlier study, we showed that the average particle radius of $Ti_{0.1}Zr_{0.9}Mn_{0.9}V_{0.1}Fe_{0.5}Ni_{0.5}$ alloy hydride after several cycles of hydrogen absorption and desorption is approximately 5 μm from the SEM image [4]. Assuming an average particle radius of 5 μm for $(Ti_{0.1}Zr_{0.9})_{1.1}Mn_{0.9}V_{0.1}Fe_{0.5}Ni_{0.5}$, the diffusion coefficients are calculated and the values are in the range 1.1×10^{-10}–5.6×10^{-10} cm^2 s^{-1}. Figure 10 shows the Arrhenius plot of $\ln k$ versus $1/T$ for the interface ($\alpha + \beta$ phase) process and $\ln D$ versus $1/T$ for the diffusion (β phase) process. Related activation energies (E_a) are obtained from the slope and the values from these measurements are $E_a = 160 \pm 10$ meV for the ($\alpha + \beta$) phase and $E_a = 210 \pm 9$ meV for the β phase. The values of the activation energy

and diffusion coefficient obtained by quasi-elastic neutron scattering for $Ti_{0.8}Zr_{0.2}CrMn$–H are 0.22–0.5 eV and $D = 6 \times 10^{-8}$ cm^2 s^{-1} at 100 K respectively [22], which are comparable to our experimental data. Earlier studies on hydrogen diffusion showed that the diffusion coefficient in $Zr(Fe_{0.3}Mn_{0.7})_2$–H is 2×10^{-11} cm^2 s^{-1} at room temperature [23]. In our previous study of kinetics of hydrogen absorption for $Ti_{0.1}Zr_{0.9}Mn_{0.9}V_{0.1}Fe_{0.5}Ni_{0.5}$, we found that $D = 2.7\times10^{-11}$ cm^2 s^{-1} at 30 °C and activation energy $E_a = 0.17$ eV in the $\alpha+\beta$ phase and 0.22 eV in the β phase [4]. The values of activation energies in $(Ti_{0.1}Zr_{0.9})_{1.1}Mn_{0.9}V_{0.1}Fe_{0.5}Ni_{0.5}$ are lower than those in $Ti_{0.1}Zr_{0.9}Mn_{0.9}V_{0.1}Fe_{0.5}Ni_{0.5}$ due to the presence of an excess amount of Zr, the most reactive element towards hydrogen.

4. Conclusion

The x-ray diffraction of $(Ti_{0.1}Zr_{0.9})_{1.1}Mn_{0.9}V_{0.1}Fe_{0.5}Ni_{0.5}$–$H_x$ with different hydrogen concentrations show that with increase of hydrogen content formation of the β phase occurs at the expense of the α phase. The *in situ* electrical resistivity measurements in $(Ti_{0.1}Zr_{0.9})_{1.1}Mn_{0.9}V_{0.1}Fe_{0.5}Ni_{0.5}$ show the presence of different phases as seen in the pressure–composition isotherms. The desorption temperature of $(Ti_{0.1}Zr_{0.9})_{1.1}Mn_{0.9}V_{0.1}Fe_{0.5}Ni_{0.5}$–$H_x$ from DSC studies is around 220 °C with hydrogen desorption from $24l(A_2B_2)$ tetrahedral sites. The kinetics of hydrogen absorption studies in $(Ti_{0.1}Zr_{0.9})_{1.1}Mn_{0.9}V_{0.1}Fe_{0.5}Ni_{0.5}$ give the activation energy and diffusion coefficient of hydrogen as 160 ± 10 meV ($\alpha + \beta$ phase), 210 ± 9 meV (β phase) and 1.1×10^{-10} cm^2 s^{-1} (30 °C) respectively.

Acknowledgments

The authors are grateful to DRDO, DST and MNES, Government of India, for supporting this work. One of the authors (MK) is grateful to IIT Madras for financial support.

References

[1] Wipf H 1997 *Hydrogen in Metals III* (*Springer Topics in Applied Physics* vol 73) (Berlin: Springer)
[2] Lee S-M, Lee H, Kim J-H, Lee P S and Lee J-Y 2000 *J. Alloys Compounds* **308** 259
[3] Zuttel A 2003 *Mater. Today* **6** 24
[4] Kandavel M and Ramaprabhu S 2003 *J. Phys.: Condens. Matter* **15** 7501–17
[5] Annapoorini S, Markandeyulu G and Rama Rao K V S 1990 *J. Phys. Soc. Japan* **59** 3014
[6] Adachi G, Niki K, Nagai H and Shiokawa J 1985 *J. Less-Common Met.* **108** 107
[7] Sakaguchi H, Yagi Y, Taniguchi N, Adachi G and Shiokawa J 1987 *J. Less-Common Met.* **135** 137
[8] Ishikawa F, Tega H, Yamamoto I and Yamaguchi M 1995 *J. Alloys Compounds* **231** 182
[9] Schlapbach L 1988 *Hydrogen in Intermetallic Compounds* vol I (Berlin: Springer) p 58
[10] Aoki K and Masumoto T 1995 *J. Alloys Compounds* **231** 20
[11] Fernandez J F, Cuevas F and Sanchez C 2000 *J. Alloys Compounds* **298** 244
[12] Aoki K, Li X-G and Masumoto T 1992 *Acta Metall. Mater.* **40** 221
[13] Rudman P S 1983 *J. Less-Common Met.* **89** 93
[14] Sivakumar R, Ramaprabhu S and Rama Rao K V S 2001 *J. Phys.: Condens. Matter* **13** 4155
[15] Joubert J-M, Latroche M, Percheron-Guegan A and Bouree-Vigneron F 1995 *J. Alloys Compounds* **217** 283–6
[16] Koh J T, Goudy A J, Huang P and Zhou G 1989 *J. Less-Common Met.* **153** 89
[17] Zarynow A, Goudy A J, Schweibenz R G and Cluy K R 1991 *J. Less-Common Met.* **172–174** 1009
[18] Wang X L and Suda S 1992 *J. Alloys Compounds* **184** 109
[19] Ramesh R and Rama Rao K V S 1993 *J. Alloys Compounds* **191** 101
[20] Crank J 1956 *Mathematics of Diffusion* (Fair Lawn, NJ: Oxford University Press)
[21] Jost W 1952 *Diffusion in Solids, Liquids and Gases* (New York: Academic)
[22] Hempelmann R, Richter D, Pugliese R and Vinhas L A 1983 *J. Phys. F: Met. Phys.* **13** 59
[23] Shitikov V, Hilscher G and Kirchmayr H 1984 *J. Less-Common Met.* **102** 29